Luffa Cylindrica as a durable biofiber reinforcement for epoxy systems

Erato Psarra, George C. Papanicolaou

Version of Record: https://www.sciencedirect.com/science/article/pii/S0266353820323885
Manuscript_c868f05f1a7479a95d3d131130fd64d4

Luffa Cylindrica as a durable biofiber reinforcement for epoxy systems[⋆,⋆⋆]

Erato Psarra[a,*], George C. Papanicolaou[b]

[a]*Interstellar Lab, Station F, 5 Parvis Alan Turing, 75013, Paris, France*
[b]*Department of Mechanical Engineering and Aeronautics, University of Patras, GR-26500, Patras, Greece*

ARTICLE INFO

Keywords:

Natural fibres

Natural fibre composites

Polymer-matrix composites (PMCs)

Creep

Material modelling

ABSTRACT

Luffa Cylindrica (LC) is the dried fruit of a sponge-type plant belonging to Curcubitacea family. Recent advancements in hierarchical and lightweight structures have aroused interest in this natural fibrous material for illustrating an extraordinary multi-porous architecture of high anisotropy and low density. To the extent of its biodegradable nature, such a structure is potentially apt to replace conventional porous-like composites for low-energy absorbing and material reinforcing applications. In order to investigate its candidacy as a long-term sustainable reinforcement, a LC layer is impregnated with an epoxy resin (ER) system and subjected to tensile creep tests within the linear viscoelastic regime. Specimens loaded with 30% weight fraction of LC fibers are tested at four stress levels corresponding to 5%, 8%, 10% and 15% of the static tensile strength σ_u of the composite. The viscoelastic response of the LC/ER composite is found improved with respect to that of the pure polymer. This improvement is reflected to the creep strain and compliance that decreased by 30%. The creep results are subsequently probed by means of the four–parameter (Burger) analytical model to gain insight on the viscoelastic behavior.

1. Introduction

Natural fiber composites (NFCs) are recently acclaimed for long-term sustainable industrialization potentials [39, 36, 9, 49]. With global warming effects lie in wait, this interest meets the needs of our times and lies in the natural reinforcements; a renewable, recyclable and earth-abundant source of material. Natural fillers satisfy environmental durability for attaining biomass biodegradability, ability to combust without producing harmful gases or solid residues, and energy recovery. In addition to their superior environmental performance [5, 76], their low density and low cost are apt to introduce them as a strong alternative for the industries associated with the composite materials [77, 61, 78, 38, 35, 48, 50, 42]. NFCs show adequate engineering performance, while meeting the requirements of structural applications such as decks, interior

erato@interstellarlab.earth (E. Psarra); gpapan@upatras.gr (G.C. Papanicolaou)
ORCID(s): 0000-0002-6272-9951 (E. Psarra)

panels, railing and automotive components [26, 36, 19, 33, 40, 54]. To this end, the investigation for novel natural materials as potential reinforcements for long-term performance is claimed crucial.

A newly known natural reinforcement is Luffa Cylindrica (LC), the dried fruit of a sponge-type plant belonging to Curcubitacea family. Common sponges vary in length from 15 cm to 60 cm, while their molecular composition consists of cellulose (60%), semi-cellulose (30%) and lignin (10%) [73, 30, 46]. The fruit holds a cylindrical shape of continuous fibers joined in a polyporous lattice complex architecture; see Figs.1a-e. Such a structure comprises a vascular interlaced system of random micro-truss networks of extremely high porosity (79-93%) [11, 12, 80, 17]. Albeit growing in different directions, the fibrous system exhibits dominant patterns: fibers grow in the longitudinal direction on the inner surface, in the circumferential direction on the outer surface, and in the radial direction within the core region; see Figs.1b,c,d.

LC sponge has all features of a typical biological product: abundance in nature, low cost, low weight, non-toxicity, physical and chemical stability during life expectancy, biodegradability after disposal in composting conditions. Such features make the material a sustainable environmental product that suggests an alternative to the scarcity of material resources. Albeit biological, LC reveals significant mechanical and energy storage properties [68, 29, 69], absorbing sound and shock waves; see applications in helmets and automobiles [75, 20]. Nevertheless, the application fields for LC are still limited, noting the major ones: textile industry, biotechnology and environmental engineering; see [44]. As a sponge, LC is worldwide spread as a scrubber for skin care. As a biomaterial [25, 63], it is suggested as a plant cell immobilization carrier and a drug-controlled release (delivery) system in wound dressing and wound healing [59, 62, 43]. Further research has indicated its candidacy as packaging biodegradable material [51], as removal adsorbent of toxic products (e.g., synthetic phenols, dyes) from aqueous solutions [22] and heavy metals (Cu2+) from industrial waters [45], as biofuel with low CO_2 emissions [6], and as car filter for diesel and steam engines [32]. In material applications, bio-nano-composites of cellulose crystals, subsequent to acid hydrolysis of LC fibers, have started gaining traction for their thermal and mechanical properties [71, 28].

In structural applications, LC is apt to be used as an effective reinforcement for lightweight composites, given its multi-porous and light structure [12, 31, 64, 18]. However, the use of the material is constrained by the deficient data on its engineering properties. Little study has been carried out on its mechanical response, comprising a static characterization of LC as reinforcing material for polymers by Papanicolaou et al. [60]. More specifically, several Luffa Cylindrica/Epoxy Resin (LC/ER) systems were prepared and subjected to

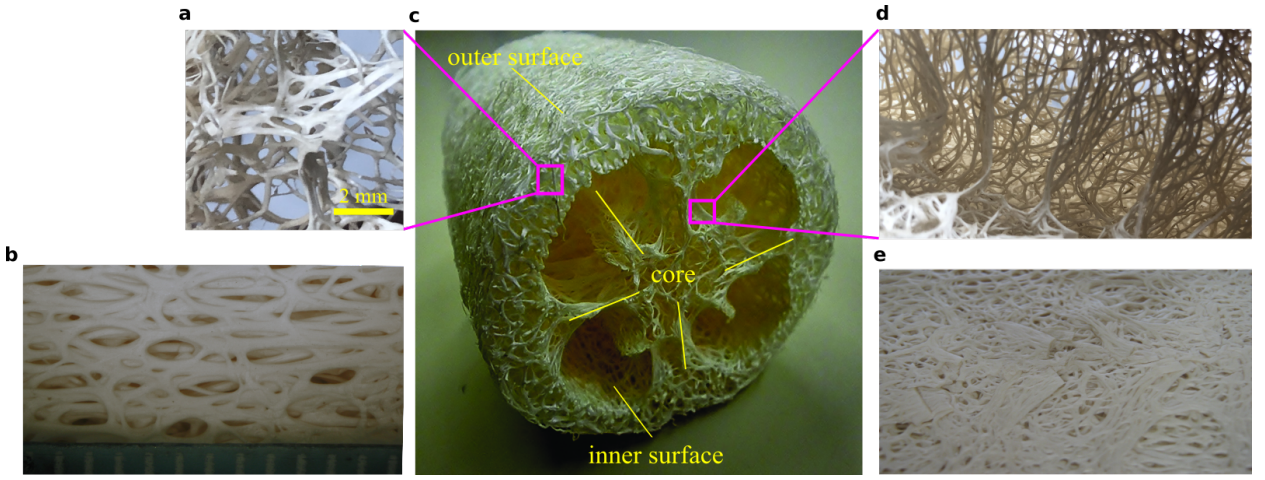

Figure 1: LC column fiber polyporous network morphology and structure: (**a**) Random macropore layer from the middle of the column wall; (**b**) The inner layer with fibers oriented along the longitudinal axis of the cylinder (**c**) Glocal view and geometrical features; (**d**) The radial core layer; (**e**) The radial core layer incorporated to the inner layer through compression, after cylinder-to-lamina shape transformation.

tensile tests, subsequent to scanning-electron microscopy (SEM) observations. The applied fabrication optimization process (i.e., chemical treatment, ply lay-up number and orientation, fiber-weight fraction, pressure conditions at curing) led to a considerable improvement of the elastic response up to 48%.

Natural fibres have generally poor interfacial adhesion with epoxy systems and chemical treatment is required. To this end, different surface treatments were tested by the authors [60], such as acetone and acidic solutions in acetone, alkali with peroxidation, acetylation and mercerization techniques. The solution of Acetone/CH_3COOH 1% was found to increase the static behavior of the composite by 30%. That first study has revealed that LC fibers present a reasonable static performance, meeting the requirements of modern applications upon the "green" reinforcement of epoxy systems [67, 66, 34, 79, 74]. However, a research gap has been noticed to exist on the long-term sustainability data, where a first comprehension of LC durability is yet to be achieved; save for [27].

To this end, static characterization cannot be claimed sufficient in terms of long-term performance under moisture effects, alkaline interactions, fatigue, creep and physical degradation [8, 48, 17]. To slightly fill the research gap on the sustainability data of polymer-based NFCs, we provide a viscoelastic (creep) characterization of an epoxy impregnated LC system. Creep is the progressive deformation of a material under constant load (stress). It is attributed to the coupling of elastic deformation and viscous flow and it is one of the first parameters to be considered when designing polymer-based composites [65, 1]. This owes to a slow

failure mechanism that may occur to a material exposed for a prolonged period to a load below its elastic limit. In the tensile creep, the material elongates in the direction of the applied load. At ambient temperature, such a deformation can be very low for metals and ceramics and, thus, not important. However, even at room temperature, the effect of creep in polymeric structural components is significant. In conjunction with the environmental conditions effects, their ultra-sensitive time-dependency is known to be a non-beneficial factor to their performance [14]. To this extent, the creep behavior of polymers has been largely explored, yet there is this gap on the time-dependent contribution of natural fibers to polymer-based composites; see [56].

To investigate the LC candidacy as a durable engineering material, the present work treats the viscoelastic experimental characterization of our lately designed semi-green LC/ER composite material. A single ply LC is impregnated with a resin system and subjected to tensile creep and recovery tests. The structural pattern of LC is exploited to create unidirectional (UDI) long-fiber specimens. We note that the present study comprises a follow-up of our publication on the structural and mechanical characterization of the LC/ER composite [60]. The interested reader in the mechanical design of the composite can refer to our primary work, where the mechanical (static) performance of LC/ER is investigated under different fabrication conditions. Here, the LC/ER composite tested under creep is that manifesting the highest mechanical properties, i.e., among samples of different fiber concentrations, orientations and distributions, as shown in our parametric study. In section 2, we present the structure of the material system, the fabrication method of the LC/ER composite and the experimental process. We note that the creep tests have been performed within the linear viscoelastic regime for 30% fiber-weight fraction specimens and under four stress levels (5%, 8%, 10% and 15% of the tensile strength of the LC/ER composite). In section 3, theoretical estimates for material parameter identification are employed to determine the viscoelastic behavior of the system at hand. Here, we give rise to the four–parameter (Burger) model for being more representational of the polymer behavior than other lower–order models. In section 4, the experimental results are presented and probed by means of the four–parameter model to gain insight into the viscoelastic response.

2. Material and methods

2.1. Materials

The matrix material of the composite is the epoxy resin system under the commercial designation Ren-Lam CY 219, Huntsman Co., Switzerland. The hardener used is the Ren HY 5161, Huntsman Co.

The LC sponges were supplied by Ningbo Kanger Greenness Consumer Co., Ltd, Ningbo, China and received in the form of dry compact layers (plies) with long continuous fibers oriented in parallel with the longitudinal direction of the layer; see Figs.2a,b. The dimensions of such plies were 200 x 130 ($\pm$10) x 2 ($\pm$0.2) mm^3. The struts within a LC layer were defined by a micro-cellular architecture of continuous hollow micro-channels (pores with diameter of 1–4 mm) that form vascular bundles and yield a multimodal pore system; see Figs.1a-e,2e. Within each layer, fibrils interlace with each other forming micro-trusses, retaining though the dominant scale-up orientation, e.g., Figs.1d,2b. The material structure within lamina is quite complex, especially after taking into account the regions where fibers grow in orientations different from the principal ones; also see Fig.2a. Such different orientations are attributed to the processing method, transforming the material from cylinder to lamina. The transformation requires a longitudinal section at the circumference of the cylinder and throughout its wall thickness. Subsequently, the developed layer is subjected to compression along the thickness, leading to the integration of the damaged core fibers into the new main in-plane body. To this end, this is how the randomly oriented regions of fibers are formed, interconnected with each other in various directions (note that two dominant directions of $[\pm 45]^{\mathrm{T}}$ can be observed nevertheless).

2.2. Sample preparation

2.2.1. Fabrication of pure epoxy resin specimens

Following a first heating up to 50°C for 2 min to decrease its viscosity, the resin pre-polymer was mixed with the hardener at a weight ratio 2:1. After being thoroughly stirred for 5 min, the mixture was degassed into a vacuum chamber for 7 min and then poured into a rectangular metallic mold. The mold was previously cleaned, polished and joined together with screws. It also comprised six casting positions for specimens, each one dimensioned as 165 x 20 x 2 mm. After assembling the mold to enclose the polymer mixture, the material was subjected to the optimal thermal processing studied in Papanicolaou et al. [60]. Such a processing calls for a mechanically applied pressure of 4.6 kPa at 50°C for 24h, with a 5°C h^{-1} rate of temperature rise (drop) from (to) ambient. In this way, the complete polymerization of the matrix material

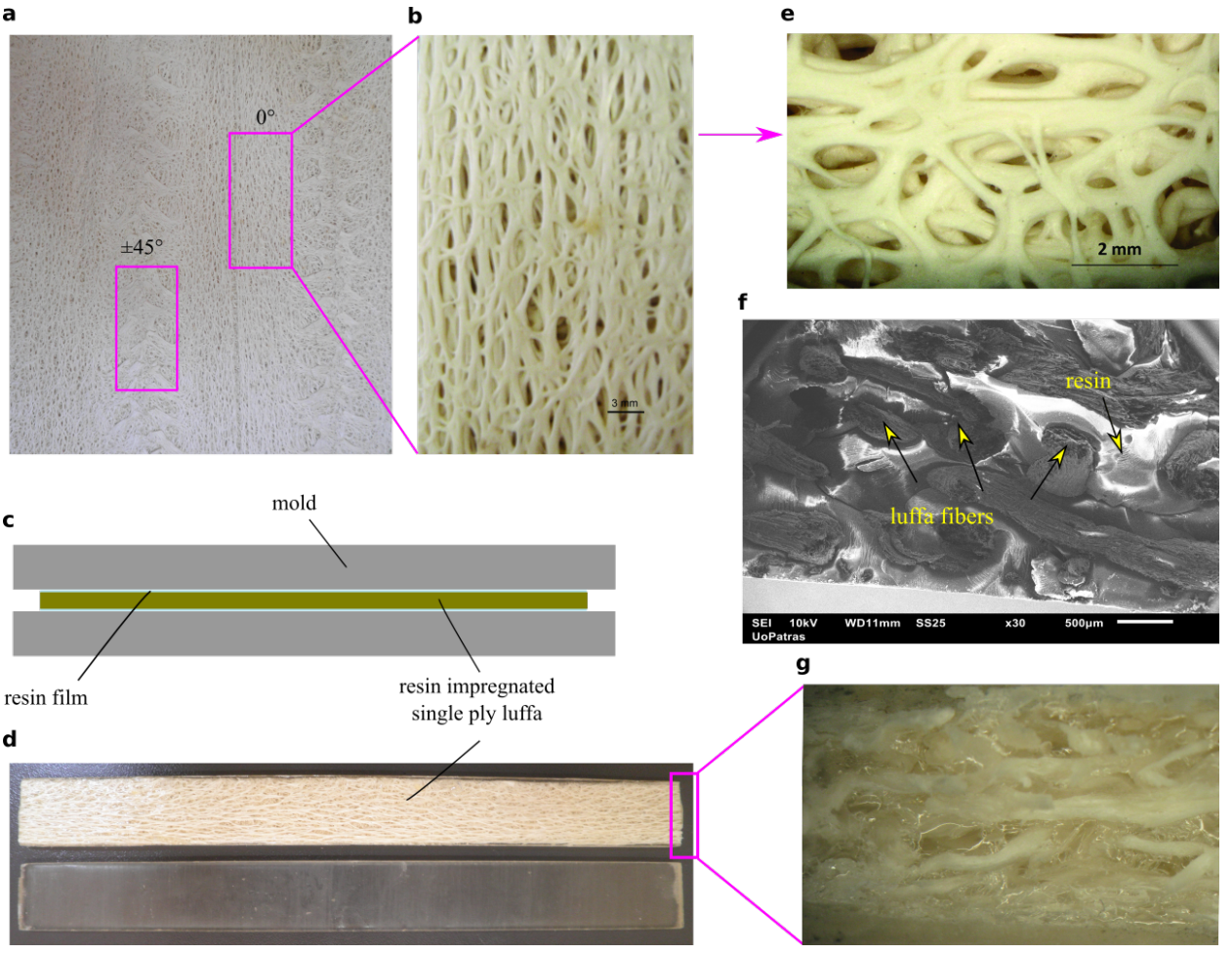

Figure 2: (**a**) Supplied LC ply sample; (**b**) Region of the LC ply with interfiber pores experimentally exploited; (**c**) Schema of fabrication setup; (**d**) A single UDI long-fiber LC ply impregnated epoxy resin (LC/ER) and a pure epoxy resin (ER) rectangular tensile creep specimen; (**e**) Continuous hollow micro-channels forming the pore system; (**f**) Scanning electron photomicrograph of a single ply LC/ER. Transverse fracture section, cross-section profiles of brittle damaged LC fibers (x30); (**g**) Optical microscopy observation of the LC/ER specimen section.

was achieved while the properties of the final product did not exhibit storage-dependence. The six creep test specimens were removed from the relevant six casting mold positions. Each specimen had dimensions 165 x 20 x 2 ($\pm$0.2) mm^3. The fabrication of the neat resin specimens was used as reference to have the prospective LC reinforcing value revealed in the next stage; see Fig.2d.

2.2.2. Fabrication of LC epoxy composite specimens

The metallic mold surfaces were carefully washed, dried and lightly waxed. The mold was subsequently joined together with screws. Six LC specimens were cut out from the raw LC plies in dimensions 165 x 20 x 2 ($\pm$0.2) (mm), strictly taken from the regions of the plies where the reinforcing fibers are in parallel; see

Figs.2a,b,d. The specimens prepared from the sheet were cut in the same direction. The resin pre-polymer was weighed out and catalyzed at a weight ratio 2:1. After stirring for 5 min, the mixture was degassed into a vacuum chamber for 7 min. As depicted in Fig.2c, a thin film of stirred mixture was applied at the bottom of the six casting positions. Six LC plies were then impregnated with resin and placed within the six casting positions. If needed, the upper surfaces of the single LC ply specimens were additionally filled with resin. Next, the system was subjected to the same 24h thermal/pressure processing of the pure polymer specimens described above (see paragraph 2.2.1). Preconditioning of the specimens prior to testing was considered for at least 48h. Since the properties can be affected by moisture, the specimens were kept in dry sealed environments. Each specimen measured 165 x 20 x 2.2 ($\pm$0.2) mm^3. The reinforcement weight fraction at 30% was calculated as W_f = (raw LC ply mass / composite LC/ER specimen mass) x 100 (%).

Based on ASTM D2990–01 [2], the surface finish is a parameter to be considered, and the specimens should be smooth and scratch free. A slight smoothing on the transverse surfaces of the specimens (where cut LC fibers can be scratchy) was done where needed, to avoid the development of edge stresses during the creep test. Optical images by means of LEICA MZ 16 stereomicroscope were then employed to review the roughness of the sectional areas; see Fig.2g. Observations with a JSM 6610 LV Scanning Electron Microscope (SEM) of several cross–sections, perpendicular to the longitudinal axis of the fibers, showed an adequate adhesion between the fibers and the polymeric matrix; see Fig.2f.

2.3. Setup and experiment

Different creep-recovery tests are conducted at stress levels percentage of the ultimate tensile strength of the material estimated from tensile tests. An experimental static stress-strain curve of these tests is useful and thus presented in Fig.3.

The creep test measures the dimensional changes of a specimen versus time under constant static load. At a constant temperature, a constant load is applied to the specimen under a selected loading configuration, such as tension, and the deformation is measured as a function of time. Here, tensile on-axis creep tests were performed within the linear viscoelastic regime of a) three pure epoxy resin (ER) specimens and b) three 30% fiber-weight fraction LC/ER specimens. The tests were carried out under four stress levels of σ_0 = 5%, 8%, 10% and 15% of the tensile strength σ_u(= 64 MPa) of the LC/ER composite material. The tensile strength was previously measured by means of an INSTRON machine, following ASTM D638–03 [3] for the resin and ASTM D3039 [4] for the composite. It is noted that based on ASTM D2990–01 [2], in creep

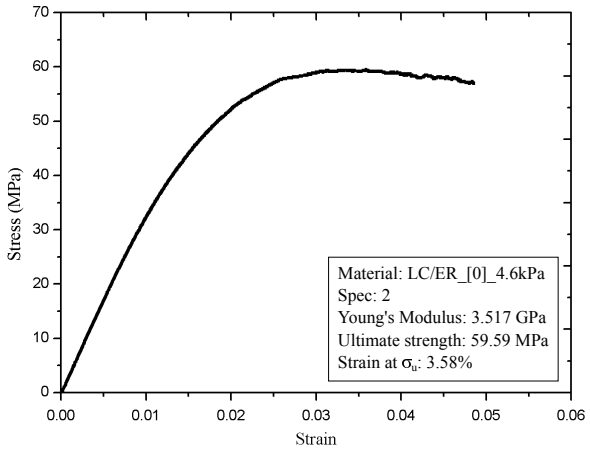

Figure 3: Experimental static test stress–strain curve of the LC/ER composite material.

testing at a single temperature, the minimum number of test specimens needed at each stress level should be three if fewer than four levels of stress are used. The specimens measured 165 x 20 x 2.2 ($\pm$0.2) mm^3, with a gauge length at 104 mm over the 165 mm of total length.

The viscoelastic characterization was carried out at a lever-armed tensile creep test machine. The initial tensile load was applied by the simple method of adding (suspending) weights to (from) the specimen. The full load was being smoothly applied to the specimen in less than 5s. The lever system was designed so that the load was kept fixed, as the lever arm was moving during the test. The ratio of the applied to the desired load was 1:4. The grips permitted the centering of the specimen prior to load application. Each test involved a 3h tensile creep loading, followed by a 3h recovery stage. The timing started at the loading onset. Upon completion of the creep stage, the load was removed rapidly and smoothly.

The extension (vertical displacement) was measured directly on the specimen by means of a Linear Variable Differential Transformer (LVDT) sensor, supplied by RDP Electronics, with 975 mV mm^{-1} sensibility. The extensometer was sensitive since the actual amount of deformation before failure was on the order of only two or three per cent. An A/D converter of the National Instruments CO was employed for the data acquisition, automatically recording displacement versus time through the LabVIEW v.60 interface. The results were then plotted on a graph of strain versus time. The measured creep strain ϵ(t), which is the total

strain at a time t produced by the applied stress during the test, was evaluated as

$$\epsilon(\mathrm{t}) = \frac{V_0 - V(\mathrm{t})}{S\ N}, \tag{1}$$

where V_0 in V the initial indication of the sensor, $V(\mathrm{t})$ in V the continuous–time signal values, S in V mm^{-1} the sensibility of the sensor and N in mm the span length of the specimen. Under constant conditions, the creep strain occurs as the response to the initial stress σ_0, which is the ratio of the applied force to the initial cross–sectional area and writes $\sigma_0 = \frac{a\ m}{A}$, with $a = 38.465$ (N kg^{-1}) the mass to load conversion coefficient, m in kg the mass of the static load, and $A = 20$ x $3 = 60$ mm^2 the area of the rectangular cross–section. For a linear viscoelastic behavior, the creep Compliance, C(t), is a time-dependent function relating the developed creep strain $\epsilon(\mathrm{t})$ to the initial applied stress σ_0 and simply writes $\mathrm{C(t)} = \frac{\epsilon(\mathrm{t})}{\sigma_0}$.

3. Theoretical analysis

3.1. Parameter estimation of the four–parameter viscoelastic (Burger) model

The linear viscoelastic behavior of a material can be represented by means of simple elements. An ideally linear elastic solid is modeled by a spring, while an ideal Newtonian fluid viscous behavior can be modeled by a dashpot. On the topic of creep behavior, there have been various models eligible in both interpreting and predicting the time-dependent response of materials. Such models comprise combinations of spring/dashpot elements. The springs represent the instantaneously recoverable elastic response, while the dashpots give rise to a viscous drag. Highly elaborated models are mostly used for soil rheological behavior predictive purposes and thus, propose higher–order systems of five to seven parameters. A simpler but effective for polymer behavior model is the four–parameter (Burger) model, including a Maxwell model (spring and dashpot in series) connected in series with a Kelvin/Voigt model (spring and dashpot in parallel). We note that such a model is applicable assuming linear viscoelasticity.

In the four–parameter model, we consider two springs $F(R_1)$, $F(R_2)$ of stiffness R_1, R_2 and two dashpots $D(n_1)$, $D(n_2)$ of Newtonian viscosity n_1 and n_2 respectively; see Fig.4a. We also consider the deformation ϵ_1 corresponding to the spring with constant R_1, the deformation ϵ_2 corresponding to the viscous damping n_1 and the deformation ϵ_3 corresponding to the Voigt mechanical analog (damping n_2 and spring R_2 in parallel).

The elements $F(R_1)$ and $D(n_1)$ are in series to serve as elements of the Maxwell model. Because of the way they are connected (in series), these two elements undergo the same stress but different strains, ϵ_1 and ϵ_2

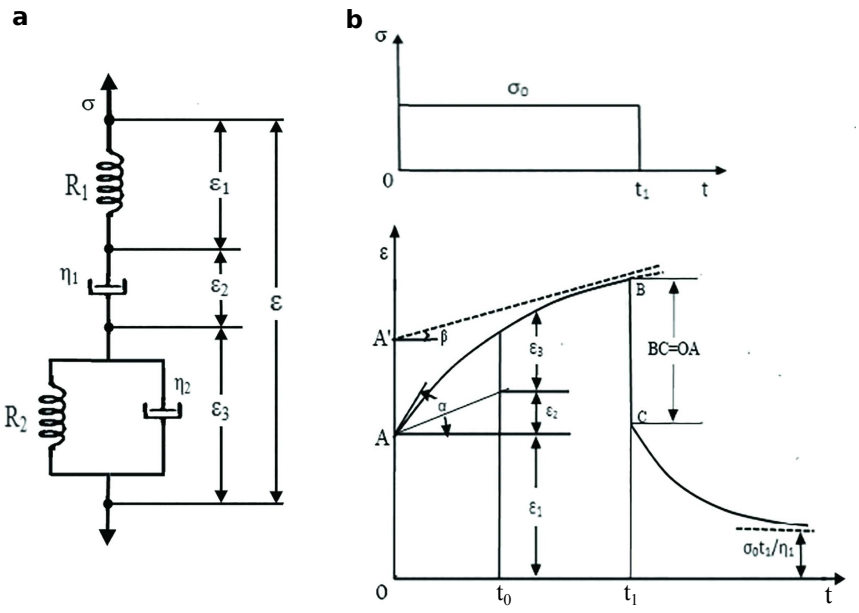

Figure 4: (**a**) Schema of the rheological four–parameter model. (**b**) Indicative creep curve for the identification of α, β, OA and AA' parameters.

respectively, see Fig.4a. The different strains at a given time t are attributed to the constitutive nature of each element: a spring deforms instantaneously, contrary to a dashpot which needs time to deform. The elements $F(R_2)$ and $D(n_2)$ are in parallel for being the elements of the Voigt model. These two elements manifest the same strain ϵ_3 but different stresses, Fig.4a. This is because their mode of connection (in parallel) forces them to deform together (isostrain condition), and under a time-dependence due to the way the dashpot functions.

To this end, the stress-strain relation of the Maxwell model writes $\sigma = R_1\epsilon_1 = n_1\dot{\epsilon_2}$, while that of the Kelvin/Voigt model writes $\sigma = R_2\epsilon_3 + n_2\dot{\epsilon_3}$.[1] Eliminating ϵ_1, ϵ_2, and ϵ_3 while applying Laplace transform, one obtains the constitutive law of the four–parameter model in terms of the total stress and strain

$$\sigma + \left(\frac{n_1}{R_1} + \frac{n_1}{R_2} + \frac{n_2}{R_2}\right)\dot{\sigma} + \frac{n_1 n_2}{R_1 R_2}\ddot{\sigma} = n_1\dot{\epsilon} + \frac{n_1 n_2}{R_2}\ddot{\epsilon}. \tag{2}$$

Solving eq.2, for $\sigma = \sigma_0 = \text{const.}$, we obtain the creep strain

$$\epsilon(\mathrm{t}) = \frac{\sigma_0}{R_1} + \frac{\sigma_0}{n_1}\mathrm{t} + \frac{\sigma_0}{R_2}\left(1 - \exp\left(\frac{-R_2\mathrm{t}}{n_2}\right)\right). \tag{3}$$

From eq.3, we observe that the creep behavior of the four–parameter model is simply the sum of the Maxwell

[1]The "over-dot" Newton notation $\dot{y}$ denotes the time derivative of y, where y is a function of t. Similarly, the second derivative of a function y of t is represented using double "over-dot" notation, $\ddot{y}$.

and the Voigt analog behaviors. In the right member of the relation, the first two terms express the instantaneous elastic deformation of the spring R_1 and the viscous flow of the damper n_1 of the Maxwell model, respectively. The third term expresses the delayed elastic behavior of the Voigt model.

The model can represent both loading and unloading behavior of a viscoelastic body. If the creep stress is removed at time $t = t_1$, one can assume that a constant stress $-\sigma_0$ is added to the system. According to the principle of Boltzmann superposition, the recovery strain $\epsilon(t)$ for $t > t_1$ is the sum of the creep strain $\epsilon(t < t_1)$ and the strain at load removal $\epsilon(t_1)$, i.e., the sum of the two independent actions. To this end, the recovery strain can be easily retrieved

$$\epsilon(t) = \frac{\sigma_0}{n_1} t_1 + \frac{\sigma_0}{R_2}\left(\exp\left(\frac{R_2 t_1}{n_2}\right) - 1\right)\exp\left(\frac{-R_2 t}{n_2}\right), \quad t > t_1. \tag{4}$$

Differentiating eq.3 with respect to time t, the creep rate of the viscoelastic material writes

$$\dot{\epsilon}(t) = \frac{\sigma_0}{n_1} + \frac{\sigma_0}{n_2}\exp\left(\frac{-R_2 t}{n_2}\right). \tag{5}$$

In practice, four randomly selected experimental data points are required for achieving the optimal solution. As illustrated in Fig.4b, one can identify the model parameters R_1, R_2, n_1, n_2 after estimating the geometrical features α, β, OA, AA' from an experimental creep curve, such as

$$\dot{\epsilon}(0^+) = \left(\frac{1}{n_1} + \frac{1}{n_2}\right)\sigma_0 = tan(\alpha) \tag{6a}$$

$$\dot{\epsilon}(\infty) = \frac{\sigma_0}{n_1} = tan(\beta) \tag{6b}$$

$$OA = \epsilon_1 = \frac{\sigma_0}{R_1} \tag{6c}$$

$$AA' = \frac{\sigma_0}{R_2}. \tag{6d}$$

The stiffness R_1 of the spring element $F(R_1)$ is obtained from the instantaneous strain ϵ_1 when a creep load is applied; see eq.6c. Related to the irreversible component of the viscoelastic deformation, the dashpot constant n_1 is obtained from the slope (equivalent to strain ϵ_2) in the steady state regime of the curve; see eq.6b. Similarly, related to the reversible component of the viscoelastic deformation, the stiffness constant R_2 is estimated from the delayed deformation $\epsilon_3((t_0) = AA' - \epsilon_2(t_0))$ by use of eq.6d. Reflecting the viscous reversible deformation in the regime where the delayed elasticity dominates, the dashpot coefficient n_2 is found with substitution of a data point of the creep curve (see eq.6a) into eq.5.

In Section 4.2, we will demonstrate the efficacy of the four–parameter model in predicting the response of viscoelastic NFCs, validated with the aid of our LC/ER single ply 30 wt% case study. A trial-and-error scheme will be employed to identify the model parameters. Once the parameters are known, a straightforward analysis can predict the system response.

4. Results and Discussion

4.1. Experimental behavior of LC epoxy composite vs. pure epoxy system

Four different low value stress levels σ_0, as compared to the tensile strength of the composite σ_u(= 64 MPa), were selected for loading the tensile creep specimens, i.e., $\sigma_0 \leq 0.15\sigma_u$, to reserve a linear viscoelastic response at room temperature. As seen in Figs.5a-d, the strain at time $t = 0^+$ occurs instantaneously upon application of the load.[2] Although this strain is elastic and thus simply proportional to the applied stress, it is important for being a considerable fraction of the allowable total strain. Therefore, it should be included in all calculations, especially in those for the creep modulus.

In Fig.5a, for a stress level at 3.2 MPa corresponding to $5\%\sigma_u$, a 27.11% decrease of the respective pure polymer creep strain is achieved. Such a favorable restriction of the creep phenomenon is attributed to the LC fibers, whose less ductile behavior leads to an overall restraint of deformation for the composite. In other words, the presence of rigid LC fibres increases creep resistance by hindering the mobility of the polymer network. In Fig.5b, under a stress level of 5.1 MPa corresponding to $8\%\sigma_u$, another drop of the creep

[2]For time $t = 0^-$, the applied stress is zero. For time $t = 0^+$, the stress jumps to a non-zero value.

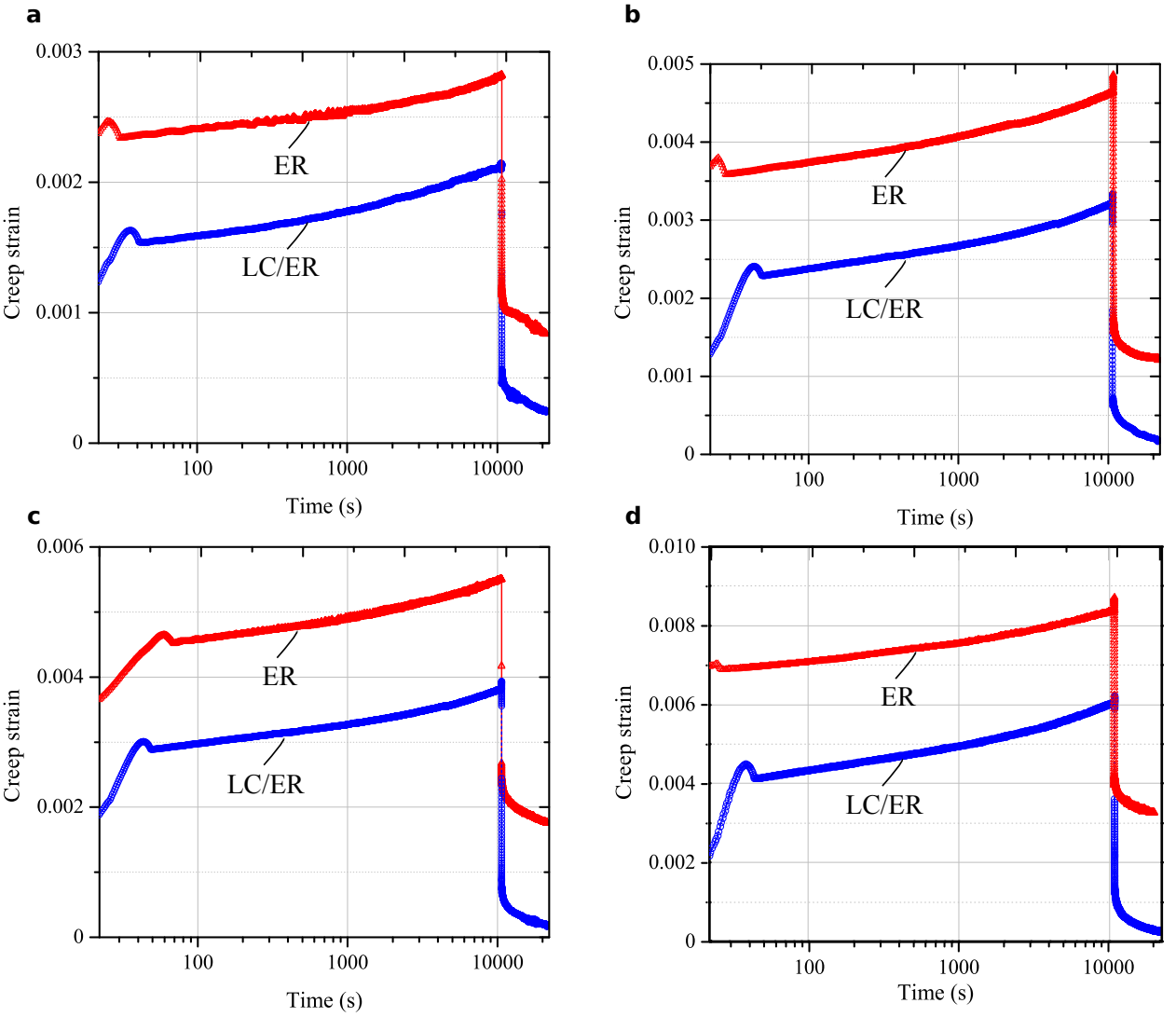

Figure 5: Tensile creep strain results for the pure resin ER and the LC/ER composite material at 25°C and stress level (**a**) $\sigma_0 = 0.05\sigma_u$; (**b**) $\sigma_0 = 0.08\sigma_u$; (**c**) $\sigma_0 = 0.1\sigma_u$; (**d**) $\sigma_0 = 0.15\sigma_u$, with σ_u the tensile strength of the LC/ER composite. The strain is plotted versus a log time axis.

strain response by 30.61% is achieved. Likewise, in Fig.5c and under a stress of 6.4 MPa corresponding to $10\%\sigma_u$, a creep strain reduction by 32.91% is attained. Eventually, in Fig.5d, under a stress level of 9.6 MPa corresponding to $15\%\sigma_u$, a nearly identical drop of 32.38% is obtained. It is noted that at each stress level, the presented percent changes in strain correspond to the arithmetic means of the experimental data points along loading, excluding the recovery part of the curves. The decrease by less than 1% of the creep percent change (or creep resistance) from the test level of $10\%\sigma_u$ to that of $15\%\sigma_u$ is shown to be attributed to the very first part of the creep curve that is susceptible to inertia phenomena; see neighborhood close to the

instant of loading imposition, t= 0^+, in Fig.5d. Such phenomena grow stronger with applying stress loading and may slightly perturb the initial slope of the curve [7],[41].

For better illustration, the creep strain behavior is shown in Figs.6a,b at a longer time t = 10000 s. In Fig.6a, the creep strain is presented versus the applied stress level for both pure resin (ER) and LC/ER composite. Here, we show the tendency of the creep response to linearly increase with applying stress. Similarly, the creep strain reduction, which simply writes the difference between ER and LC/ER strain, is shown to increase with applying stress in Fig.6b. This implies that the greater the applied load, the greater the effect of the LC fibers to restrain creep. Considering this creep restraint in percent change (i.e., resistance) in Fig.6b, the creep resistance reads 24.82%, 28.33%, 30.66% and 30.9% under a stress level of 5%, 8%, 10% and 15%σ_u, respectively. Thus, at longer times, the resistance increases with applying stress, though under a decreasing rate within the tested range of stresses $\sigma_0 > 0.1\sigma_u$, probably due to the introduction of stronger inertia phenomena at the instantaneous loading onset versus increasing stress level [7],[41] (but see also result interpretation in Section 4.2).

Another reason for such a behavior at applied stress $\sigma_0 > 0.1\sigma_u$ could be the introduction of inelastic deformations if the applied load σ_0 was close to the yield limit [37]. Then, one could capture apparent drops of creep strain, as the real strains would be underestimated due to plastic effects [55]. However, the static load

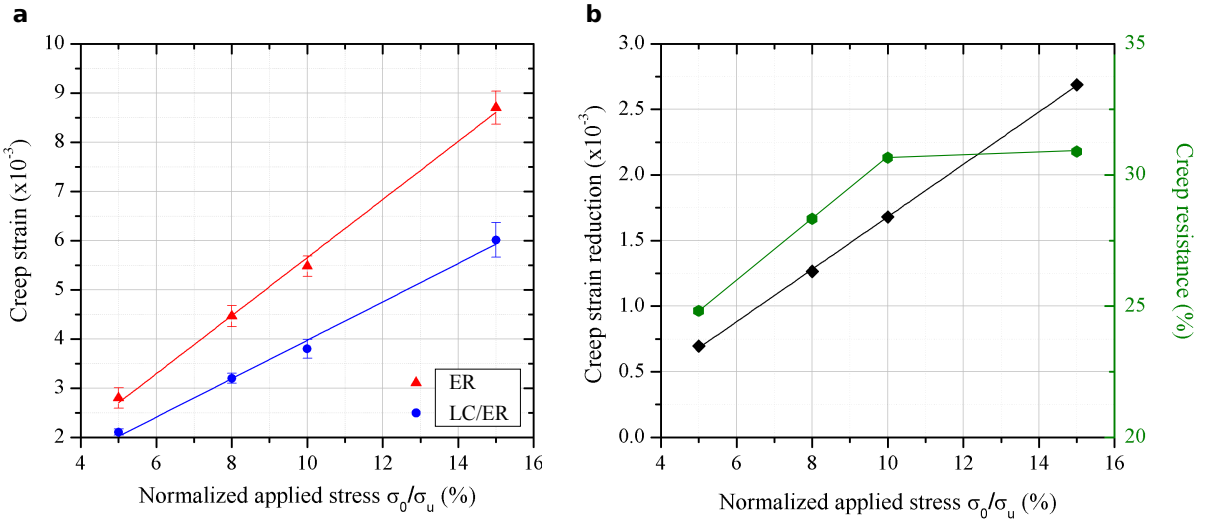

Figure 6: Tensile creep results against the normalized applied stress at 25°C and time t = 10000 s. (**a**) Creep strain for both pure resin ER and LC/ER composite. Standard deviation of measurements among three specimens is included in the experimental data points; (**b**) Creep strain reduction and creep resistance (i.e., the creep restraint in percent change) due to the LC reinforcement.

is far below the yield stress (see Fig.3) and, thus, one cannot claim that inelastic deformations have begun to act. The micro-mechanics of the composite structure [10] to restrain the viscoelastic/plastic response are presented just below. A further insight on this point will be provided by means of the viscoelastic modeling in Section 4.2.

As it is challenging to find data on LC creep response, a comparison with similar studies on other natural fibre polymer composites gives a tangible sense of the results obtained. We should note that comparisons are not direct though, due to differences in experimental conditions. Creep data at 20°C of pure polypropene (PP) and 26 wt% woodflour/PP composite report a reduction in the creep strain of woodflour/PP by about 10% compared to pure PP [53]. Another study [47] at 20% static loading level reports a creep reduction by about 18% for 30 wt% woodflour/PPcomposite. Flexural creep tests at a stress level of 5 MPa and 25°C of pure unsaturated polyester (UPE) and 10 vt% (corresponding to two reinforcing plies) hemp/UPE composites report a reduced creep strain by about 47% for the composite [23]. Injection-moulded 30 wt% short basalt fibre reinforced polylactic acid (PLA) composites showed a creep strain reduction by 24% compared to pure PLA, at 20% static loading level [72]. At 50°C, 25 wt% jute/PP composite showed a reduction by about 30% for 1 MPa constant stress [15]. We note that jute fibers are known to have much higher mechanical properties than LC fibers [58, 60], same for the sisal [58, 60]. The creep strain of 30 wt% sisal fibre reinforced PCL-starch composite is about 75% reduced compared to pure PCL-starch, for 5 MPa stress level and 28°C [21].

To gain some insight on the physical mechanism of creep restriction, the composite material can be treated as a network of chains bridged by cross-linked junctions. In a meso-scale level, this network is interpreted as a whole of meso-regions with arbitrary shapes and sizes. In relation to the theory of cooperative relaxation [10], the viscoelastic behavior owes to the rearrangement of meso-domains that occurs at random times when the regions are thermally activated. Referring to the creep behavior, polymer fiber composites can exhibit substantial creep resistance due to the restricted motion of meso-regions, derived by the presence of the fibers and the consequent creation of new adhesive bonds. These bonds depend, in turn, on the quality of the interface between the fibers and the polymeric matrix [24]. The optimized fabrication illustrated in Papanicolaou et al. [60] assures an adequately strong interfacial bonding, so that the loads can be transferred from the matrix to the fibers. To this end, the fibers manage to increase the resistance to cooperative chain segmental mobility of the polymeric chains and stiffen the matrix.

We note that no significant debonding has taken place for small times, $t \leq 40$s in Figs.5a-d. If that was the

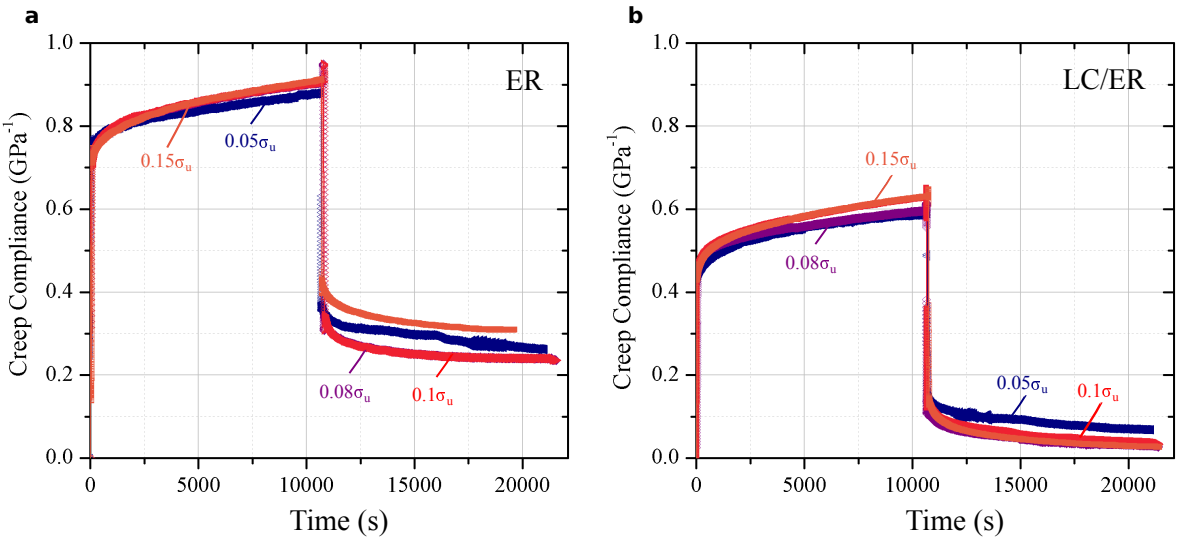

Figure 7: Tensile creep compliance curves for different stress levels at 25°C corresponding to (**a**) the pure resin ER and (**b**) LC/ER composite. Confirmation of linear viscoelasticity.

case, one could only see the resin properties prevail (at $t = 0^+$, the elastic jump of the LC/ER curves would not deviate by more than 2% from that of the pure ER polymer in Figs.5a-d [70, 57]) and other failure features would appear, e.g., long pullout lengths, neat fiber beads, etc [13]. We also note that the creep at low stress in LC fibres direction was perceivable without optically detecting damage. For porous viscoplastic materials, the damage evolution is related to the progressive debonding of the fillers and the consequent propagation of microvoids [81, 16, 70]. To estimate the macroscopic viscoplastic behavior, homogenization schemes are employed, usually under the assumption that the debonded inclusions are regarded as microvoids upon partial separation from the matrix [16, 70]. Within this framework, porous materials, such as geomaterials containing pores and rigid inclusions, e.g., claystones, have been reported to manifest debonding for times $t < 3s$ [16] and macroscopic strains $\epsilon \approx 0.01 - 0.02$ [16, 70], depending on the stress level, the size and morphology of the fillers.

To better explain debonding in monotonic loadings, strain is accumulated around the voids and defects that are randomly distributed into the volume of the deformed body. The total evolved deformation is distributed inhomogeneously around these regions, depending on the topological nature of each defect. When the distributed elastic energy (associated with this strain) of each such region reaches a critical value, an irreversible transition takes place and induces plastic deformation [52]. In the LC/ER composites though, the natural fibers are adequately adhered to the matrix due to fabrication under optimized pressure and thus,

they reduce the irreversible plastic transitions.

When being in the linear viscoelastic regime, the successive compliance moduli versus time for different stresses should superimpose upon each other; see verification in Figs.7a,b for both pure resin (ER) and LC/ER composite. The physical context of the creep compliance decrease is related to the rise of the material's difficulty to deform. Treating creep in terms of the linear viscoelastic behavior, we also present the creep test data given in Figs.5a-d manipulated by cutting sections through the creep curves at constant times and plotting the stress as a function of strain, so as to be displayed as short-term stress-strain curves. These manipulated creep curves are called isochronous curves, while their slope is defined as the creep modulus E_{creep}. It should be mentioned that if isochronous are linear this is a clear indication that the viscoelastic behavior of the materials tested is a linear viscoelastic one.

In Fig.8a, the applied stress is plotted against the developed creep strain for the LC reinforced epoxy systems, at times t = 0, 2500, 5000, 7500 s. Apart from illustrating the viscoelastic response of our materials, the isochronous plots can also serve to interpolate non-experimental data. In Fig.8b, the slopes of the isochronous curves are plotted versus time for the pure epoxy and the LC reinforced epoxy system. As expected, creep modulus variation with time follows an exponential decay.

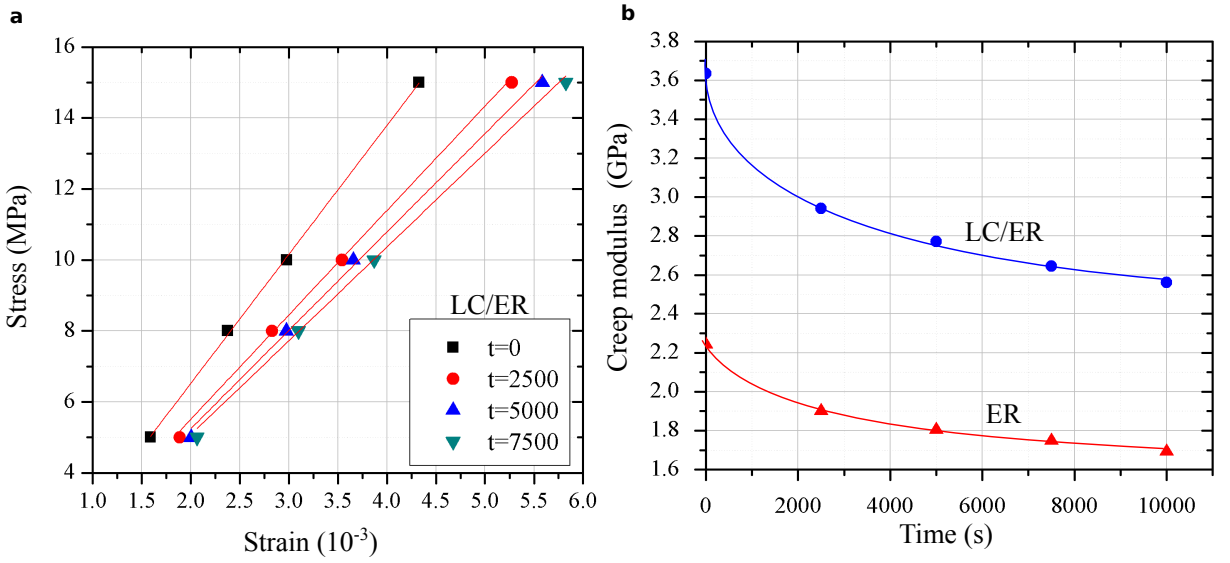

Figure 8: Constant time cross–sections (**a**) Isochronous curves for different time instants t=0,2500,5000,7500 s of LC/ER composite. (**b**) Creep Modulus of pure resin ER and LC/ER versus time.

4.2. Viscoelastic modeling of LC epoxy composite by means of the four–parameter model

The linear viscoelastic behavior of the LC/ER composite is demonstrated by the isochronous stress-strain curves in Fig.8. This satisfies the condition needed for the four-parameter (Burger) model to be applied. Model parameter estimation is of outstanding importance for correctly describing the viscoelastic behavior of a material. Although the four–parameter model is more representational of the polymer behavior than lower–order models, its use for descriptive purposes has faced challenges for determining the material parameters in real case studies. Here, we make use of the model to understand better the creep response of our LC/ER single ply 30 wt% material. Thus, our study will end with the fitting analysis after considering material parameters.

To begin with, four randomly selected experimental data points are required for achieving the optimal solution. Here, a trial-and-error scheme is employed to identify the material parameters. Once the parameters are known, a straightforward analysis can predict the system response. However, since the experimental creep curves of the $0.15\sigma_u$ applied stress level do not follow the rest of the trend, a second set of fitted values is demonstrated for this specific case. Tables 1 and 2 present the fitted values of the two curves used in correspondence to the four–parameter model intrinsic constants.

As seen in Table 1, the elastic parameter R_1 is constant irrespectively of the stress levels, demonstrating the linear elastic behavior of the model at the time of load imposition. A similar to Young's modulus behavior is rather expected, since R_1 parameter represents the reversible elastic component of the strain. Reacting instantaneously to the applied load at time $t = 0^+$, the spring $F(R_1)$ of the Maxwell model counterpart is the only element in the entire model representing elasticity. For stresses beyond the yield limit, parameter R_1 would be no longer stable, as the introduction of plastic strains would rather alter the elastic behavior of the spring.

Viscous flow expresses internal inertia that get intensified with load increase. Related to the experimental response in Section 4.1, the presence of inertia effects at small times is demonstrated through the behavior of the viscous component n_1. The parameter n_1 represents the damping behavior of the Maxwell model counterpart which is found to increase with applying load. The higher the load, the stronger the reaction of the dashpot against the load and thus, the higher the viscosity n_1. At time $t = 0^+$, although the damper $D(n_1)$ is attached in series to the other elements and can be freely deformed, it is not designed to respond to the instantaneous load imposition ($n_1 \to \infty$). Therefore, its deformation becomes gradually apparent for

Stress level σ_0 ($\%\sigma_u$)	Strain ϵ_0 (%)	$R_1 = \sigma_0/\epsilon_0$ (GPa)	$\tan(\beta)$ (1/s)	$\tan(\alpha)$ (1/s)	$n_1 = \sigma_0/\tan(\beta)$ (GPa s)	$n_2 = \sigma_0/(\tan(\alpha) - \tan(\beta))$ (GPa s)
≤ 10	0.310	2.045	1.7122e-08	4.0575e-07	2.75e+05	1.206e+04
15	0.310	2.081	2.72818e-08	7.15565e-07	3.52e+05	1.40e+04

Table 1
Geometry α, β (rad) and material R_1, n_1, n_2 parameters of the single ply LC/ER composite material of 30% fiber-weight employed in the four–parameter model analysis to probe the experimental creep curves.

Stress level σ_0 ($\%\sigma_u$)	t_i	$\epsilon(t_i)$	OA' = $\epsilon(t_i) - \tan\beta\ t_i$	AA' = OA'-ϵ_0	$R_2 = \sigma_0$/AA' (GPa)
≤ 10	10288.4	0.00308	0.00290	0.00055	8.507
15	10560.54	0.00654	0.00625	0.00163	5.9

Table 2
Geometry OA', AA' and material R_2 parameters of the single ply LC/ER composite material of 30% fiber-weight employed in the four–parameter model analysis to probe the experimental creep curves.

$t > 0^+$. Such a constitutive behavior explains the first perturbed regime of the experimental creep strain curves for $t \leq 40$s in Figs.5a-d.

Shown in Table 2, the element $F(R_2)$ represents the delayed elastic deformation of the model via the spring constant R_2 of Voigt counterpart. This spring responds to the applied static load with some phase difference, since it is in parallel connected to the damper $D(n_2)$. The damper manifests an intrinsic delayed response and binds the $F(R_2)$ spring to common deformation. As seen in the table, the parameter R_2 exhibits a notable drop from the test levels $\sigma_0 \leq 10\%\sigma_u$ to the level of $\sigma_0 = 15\%\sigma_u$. Such a variation reveals the influence of the applied load on the under-competition elastic and viscous component. At low stresses, the Voigt system is “locked" by the dashpot’s viscosity and the elastic response is dominant. Past a stress level ($\sigma_0 > 0.1\sigma_u$), the internal flow starts becoming favored until the viscous character of the material overtakes the elastic one, which gradually diminishes.

The damping element of the Voigt component $D(n_2)$ represents the flow related to the delayed viscoelastic deformation. At time $t = 0^+$, the damper is “locked" by infinite viscosity ($n_2 \to \infty$) due to inertia. A lower loading rate would reduce the viscosity of the flow and consequently the spring stiffness (since the spring is forced to follow the movement of the damper). To this end, we note that the material parameters are not constant, as they depend on the rate of the applied loading. Table 1 shows that the variation of the parameter n_2 versus stress acts in a complementary fashion to that of the parameter R_2. Voigt stiffness R_2 is constant for $\sigma_0 \leq 0.1\sigma_u$, while subsequently decreases as the viscous coefficient n_2 increases and stabilizes

(at time $\tau_{ret} = n_2/R_2$).

The retardation time τ_{ret} is the time needed for the viscous component of the behavior to become dominant. Practically, it is the time needed for the creep strain to approach a horizontal asymptote, where $\epsilon =$ const. for any time. The physical context of this time is related to the microstructure of the material. It reveals the time required for the molecules to be rearranged in the direction of the externally imposed load. Each molecule is in a different orientation with respect to the load, so it has a different delay time. Therefore, this time is not a fixed value, but a continuous distribution range.

Related to the experimental response in Section 4.1, the presence of highly viscous effects taking precedence over the elastic ones with applying load is demonstrated through the behavior of the parameters R_2 and n_2. We also observe that the coefficient n_2 is lower than that of n_1. This is because the damper $D(n_2)$ shares the applied stress with the spring $F(R_2)$, while the damper $D(n_1)$ is forced to hold the entire load by itself. Consequently, the reaction of the damper $D(n_1)$ against the external load is greater than that of the damper $D(n_2)$. Such a feature explains why the viscous flow (n_2) versus applying load does not significantly affect the initial regime of the experimental creep curves (attributed to internal inertia, see Figs.5a-d), i.e., these regimes do not significantly augment versus applying load.

Solving for the creep and the recovery response of the model (see eq.3 and 4), after defining the initial conditions and the geometrical features of a single experimental curve under $\sigma_0 = 5\%\sigma_u$ applied stress (see eq.6a-d), one has all the necessary elements to apply the model on the rest of the experimental data. In Fig.9, the theoretical and the experimental creep curves are presented together for all stress levels experimentally tested. The theoretical creep curves, generated by means of the material constants found from the stress creep tests, showed a closed agreement with the experimental data. The model is found valid to predict the developed strain versus time for the entire range of the applied stress levels $\sigma_0 \leq 10\%\sigma_u$, except of the case of $\sigma_0 = 15\%\sigma_u$ which diverges from the main trend of the response and thus, requires its own set of material parameters. The model can represent both the loading and the unloading behavior of our LC/ER composite. However, the efficacy of the developed procedure in back-estimating the model parameters has been demonstrated considering only the loading phase. A less precise recovery description is observed, mostly for the stress level of $15\%\sigma_u$, caused by the challenges at the instant of load removal.

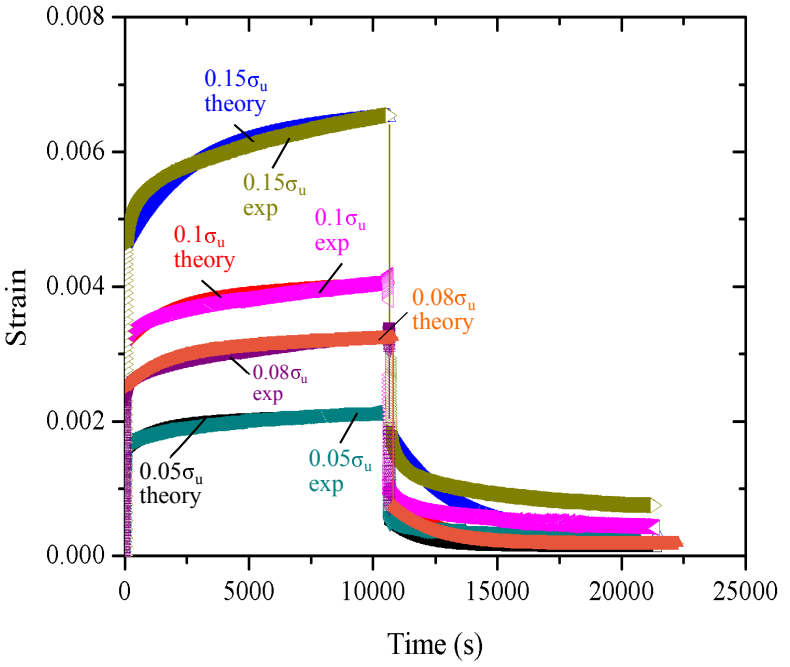

Figure 9: Fitting the experimental LC/ER creep curves with the four–parameter model under tested stress levels $\sigma_0 = 0.05, 0.08, 0.1, 0.15\sigma_u$, with σ_u the tensile strength of the LC/ER composite.

5. Conclusions

To investigate the candidacy of the natural fibrous Luffa Cylidrica (LC) as a durable engineering material for lightweight structural applications, this work presents the viscoelastic (creep) characterization of our newly designed semi-green LC epoxy composite. Given the urge to find alternatives towards the scarcity of material resources, LC biomaterial exhibits properties that are worth to be studied. The use of LC fibre reinforced composites in engineering applications is merely considered and a thorough comprehension of their durability is yet to be achieved. Here, we tackle the restriction of the creep response, since it is a phenomenon costing performance of polymers under real operating conditions. The natural fibers LC are found efficient in restricting the creep behavior of the epoxy system, providing a higher by 30% performance. The present study suggests a very first step towards the tensile creep characterization of LC thermoset composites. The effect of temperature combined with surface treatment on LC creep is a next step to consider.

Acknowledgments

This research did not receive any specific grant from funding agencies in the public, commercial, or not-for-profit sectors.

References

[1] Abdel-Magid, B., Lopez-Anido, R., Smith, G., Trofka, S., 2003. Flexure creep properties of e-glass reinforced polymers. Composite Structures 62, 247 – 253. URL: http://www.sciencedirect.com/science/article/pii/S0263822303002617, doi:https://doi.org/10.1016/j.compstruct.2003.09.022.

[2] ASTM, 2001. D2990-01 standard test methods for tensile, compressive, and flexural creep and creep-rupture of plastics. ASTM International, West Conshohocken, PA URL: www.astm.org, doi:10.1520/D2990-01.

[3] ASTM, 2003. D638-03 standard test method for tensile properties of plastics. ASTM International, West Conshohocken, PA URL: www.astm.org, doi:10.1520/D0638-03.

[4] ASTM, 2017. D3039 standard test method for tensile properties of polymer matrix composite materials. ASTM International, West Conshohocken, PA URL: www.astm.org, doi:10.1520/D3039_D3039M-17.

[5] Augier, L., Sperone, G., Vaca-Garcia, C., Borredon, M.E., 2007. Influence of the wood fibre filler on the internal recycling of poly(vinyl chloride)-based composites. Polymer Degradation and Stability 92, 1169 – 1176. URL: http://www.sciencedirect.com/science/article/pii/S0141391007001425, doi:https://doi.org/10.1016/j.polymdegradstab.2007.04.010.

[6] Bamgboye, A., Oniya, O., 2012. Fuel properties of loofah (luffa cylindrica l.) biofuel blended with diesel. African Journal of Environmental Science and Technology 6, 1–10. doi:10.5897/AJEST11.364.

[7] Baravian, C., Quemada, D., 1998. Using instrumental inertia in controlled stress rheometry. Rheologica Acta 37, 223–233.

[8] Bledzki, A.K., Faruk, O., 2004. Creep and impact properties of wood fibre-polypropylene composites: influence of temperature and moisture content. Composites Science and Technology 64, 693 – 700. URL: http://www.sciencedirect.com/science/article/pii/S0266353803002914, doi:https://doi.org/10.1016/S0266-3538(03)00291-4.

[9] Bogoeva-Gaceva, G., Avella, M., Malinconico, M., Buzarovska, A., Grozdanov, A., Gentile, G., Errico, M.E., 2007. Natural fiber eco-composites. Polymer Composites 28, 98–107. URL: https://onlinelibrary.wiley.com/doi/abs/10.1002/pc.20270, doi:10.1002/pc.20270, arXiv:https://onlinelibrary.wiley.com/doi/pdf/10.1002/pc.20270.

[10] Bohlin, L., 1980. A theory of flow as a cooperative phenomenon. Journal of Colloid and Interface Science 74, 423 – 434. URL: http://www.sciencedirect.com/science/article/pii/0021979780902118, doi:https://doi.org/10.1016/0021-9797(80)90211-8.

[11] Bou-Saab, H., Boulanger, A., Schellenbaum, P., Neunlist, S., 2013. Performance of luffa cylindrica as immobilization matrix in bioconversion reactions by nicotiana tabacum by-2. Journal of Bioscience and Bioengineering 116, 506 – 508. URL: http://www.sciencedirect.com/science/article/pii/S1389172313001564, doi:https://doi.org/10.1016/j.jbiosc.2013.04.017.

[12] Boynard, C.A., d'Almeida, J.R.M., 2000. Morphological characterization and mechanical behavior of sponge gourd (luffa cylindrica)-polyester composite materials. Polymer-Plastics Technology and Engineering 39, 489–499. URL: https://doi.org/10.1081/PPT-100100042, doi:10.1081/PPT-100100042, arXiv:https://doi.org/10.1081/PPT-100100042.

[13] Boynard, C.A., Monteiro, S.N., d'Almeida, J.R.M., 2003. Aspects of alkali treatment of sponge gourd (luffa cylindrica) fibers on the flexural properties of polyester matrix composites. Journal of Applied Polymer Science 87, 1927–1932. URL: https://onlinelibrary.wiley.com/doi/abs/10.1002/app.11522, doi:10.1002/app.11522, arXiv:https://onlinelibrary.wiley.com/doi/pdf/10.1002/app.11522.

[14] Brinson, H.F., 1999. Matrix dominated time dependent failure predictions in polymer matrix composites. Composite Structures 47, 445 – 456. URL: http://www.sciencedirect.com/science/article/pii/S0263822300000751, doi:https://doi.org/10.1016/S0263-8223(00)00075-1. tenth International Conference on Composite Structures.

[15] Chandekar, H., Chaudhari, V., 2016. Flexural creep behaviour of jute polypropylene composites. IOP Conf. Ser.: Mater. Sci.Eng. 149.

[16] Chen, J.K., ping Huang, Z., Yuan, M., 2008. A constitutive theory of particulate-reinforced viscoelastic materials with partially debonded microvoids. Computational Materials Science 41, 334–343.

[17] Chen, Y., Su, N., Zhang, K., Shiliu, Z., Zhu, Z., Qin, W., Yang, Y., Shi, Y., Fan, S., Wang, Z., Guo, Y., 2018a. Effect of fiber surface treatment on structure, moisture absorption and mechanical properties of luffa sponge fiber bundles. Industrial Crops and Products 123, 341–352. doi:10.1016/j.indcrop.2018.06.079.

[18] Chen, Y., Yuan, F., Guo, Y., Hu, D., Zhu, Z., Zhang, K., Shiliu, Z., 2018b. A novel mattress filling material comprising of luffa fibers and eva resin. Industrial Crops and Products 124, 213–215. doi:10.1016/j.indcrop.2018.07.074.

[19] Cheung, H., po Ho, M., tak Lau, K., Cardona, F., Hui, D., 2009. Natural fibre-reinforced composites for bioengineering and environmental engineering applications. Composites Part B: Engineering 40, 655 – 663. URL: http://www.sciencedirect.com/science/article/pii/S1359836809000730, doi:https://doi.org/10.1016/j.compositesb.2009.04.014. natural fiber composites.

[20] Contreras-Andrade, I., Rincon-Pardo, D., Guerrero-Fajardo, C.A., Parra-Santiago, J., Guerrero-Romero, E., 2014. Natural composite material from steelwool or luffa cylindrica under natural, rigid and flexible resin. J Chem Chem Eng 8, 906–917. doi:doi:10.17265/1934-7375/2014.09.010.

[21] Cyras, V., Martucci, F., Iannace, S., Vasquez, A., 2002. Influence of the fiber content and theprocessing conditions on the flexuralcreep behavior of sisalâĂŞpclâĂŞstarchcomposites. Journal ofTHERMOPLASTICCOMPOSITEMATERIALS, 15, 253–265.

[22] Demir, H., Top, A., Balkose, D., Ulku, S., 2008. Dye adsorption behavior of luffa cylindrica fibers. Journal of Hazardous Materials 153, 389 – 394. URL: http://www.sciencedirect.com/science/article/pii/S0304389407012435, doi:https://doi.org/10.1016/j.jhazmat.2007.08.070.

[23] Dhakal, H.N., Zhang, Z.Y., Richardson, M.O.W., 2009. Creep behaviour of natural fibre reinforced unsaturated polyester composites. Journal of Biobased Materials and Bioenergy 3, 232âĂŞ237.

[24] Drozdov, A.D., de Christiansen, J., 2003. The effect of annealing on the elastoplastic and viscoelastic responses of isotactic polypropylene. Computational Materials Science 27, 403–422.

[25] Du, Q., Cui, H., 2007. A new flavone glycoside from the fruits of luffa cylindrica. Fitoterapia 78, 609 – 610. URL: http://www.sciencedirect.com/science/article/pii/S0367326X07001761, doi:https://doi.org/10.1016/j.fitote.2007.05.004.

[26] Dweib, M., Hu, B., O'Donnell, A., Shenton, H., Wool, R., 2004. All natural composite sandwich beams for structural applications. Composite Structures 63, 147 – 157. URL: http://www.sciencedirect.com/science/article/pii/S0263822303001430, doi:https://doi.org/10.1016/S0263-8223(03)00143-0.

[27] Escocio, V.A., Pacheco, E.B.A.V., da Silva, A.L.N., de Paula Cavalcante, A., Visconte, L.L.Y., 2015. Rheological behavior of renewable polyethylene (hdpe) composites and sponge gourd (luffa cylindrica) residue. International Journal of Polymer Science URL: https://www.hindawi.com/journals/ijps/2015/714352/.

[28] Follain, N., Belbekhouche, S., Bras, J., Siqueira, G., Marais, S., Dufresne, A., 2013. Water transport properties of bio-nanocomposites reinforced by luffa cylindrica cellulose nanocrystals. Journal of Membrane Science 427, 218 – 229. URL: http://www.sciencedirect.com/science/article/pii/S0376738812007326, doi:https://doi.org/10.1016/j.memsci.2012.09.048.

[29] Genc, G., 2015. Dynamic properties of luffa cylindrica fiber reinforced bio-composite beam. Journal of Vibroengineering 17, 1615–1622. URL: https://www.jvejournals.com/article/15890.

[30] Ghali, L., Msahli, S., Zidi, M., Sakli, F., 2009. Effect of pre-treatment of luffa fibres on the structural properties. Materials Letters 63, 61 – 63. URL: http://www.sciencedirect.com/science/article/pii/S0167577X08007647, doi:https://doi.org/10.1016/j.matlet.2008.09.008.

[31] Ghali, L., Msahli, S., Zidi, M., Sakli, F., 2011. Effects of fiber weight ratio, structure and fiber modification onto flexural properties of luffa-polyester composites. Advances in Materials Physics and Chemistry 1, 78–85. URL: https://file.scirp.org/pdf/AMPC20110300005_74860202.pdf.

[32] Ghobadian, B., Rahimi, H., Nikbakht, A., Najafi, G., Yusaf, T., 2009. Diesel engine performance and exhaust emission analysis using waste cooking biodiesel fuel with an artificial neural network. Renewable Energy 34, 976 – 982. URL: http://www.sciencedirect.com/science/article/pii/S0960148108003108, doi:https://doi.org/10.1016/j.renene.2008.08.008.

[33] Graupner, N., Herrmann, A.S., Mussig, J., 2009. Natural and man-made cellulose fibre-reinforced poly(lactic acid) (pla) composites: An overview about mechanical characteristics and application areas. Composites Part A: Applied Science and Manufacturing 40, 810 – 821. URL: http://www.sciencedirect.com/science/article/pii/S1359835X09000840, doi:https://doi.org/10.1016/j.compositesa.2009.04.003.

[34] Harish, S., Michael, D.P., Bensely, A., Lal, D.M., Rajadurai, A., 2009. Mechanical property evaluation of natural fiber coir composite. Materials Characterization 60, 44 – 49. URL: http://www.sciencedirect.com/science/article/pii/S1044580308001861, doi:https://doi.org/10.1016/j.matchar.2008.07.001.

[35] Herrera-Franco, P., Valadez-Gonzalez, A., 2005. A study of the mechanical properties of short natural-fiber reinforced composites. Composites Part B: Engineering 36, 597 – 608. URL: http://www.sciencedirect.com/science/article/pii/S1359836805000442, doi:https://doi.org/10.1016/j.compositesb.2005.04.001.

[36] Holbery, J., Houston, D., 2006. Natural-fiber-reinforced polymer composites in automotive applications. JOM 58, 80–86. URL: https://doi.org/10.1007/s11837-006-0234-2, doi:10.1007/s11837-006-0234-2.

[37] Ishai, O., Bodner, S.R., 1970. Limits of linear viscoelasticity and yield of a filled and unfilled epoxy resin. Transactions of the Society of Rheology 14. doi:https://doi.org/10.1122/1.549189.

[38] Jacob, M., Thomas, S., Varughese, K., 2004. Mechanical properties of sisal/oil palm hybrid fiber reinforced natural rubber composites. Composites Science and Technology 64, 955 – 965. URL: http://www.sciencedirect.com/science/article/pii/S0266353803002616, doi:https://doi.org/10.1016/S0266-3538(03)00261-6.

[39] Joshi, S., Drzal, L., Mohanty, A., Arora, S., 2004. Are natural fiber composites environmentally superior to glass fiber reinforced composites? Composites Part A: Applied Science and Manufacturing 35, 371 – 376. URL: http://www.sciencedirect.com/science/article/pii/S1359835X03002951, doi:https://doi.org/10.1016/j.compositesa.2003.09.016. aIChE 2002.

[40] Kalia, S., Kaith, B., Kaur, I., 2009. Pretreatments of natural fibers and their application as reinforcing material in polymer composites-a review. Polymer Engineering & Science 49, 1253–1272. URL: https://onlinelibrary.wiley.com/doi/abs/10.1002/pen.21328, doi:10.1002/pen.21328, arXiv:https://onlinelibrary.wiley.com/doi/pdf/10.1002/pen.21328.

[41] Kim, M., Bae, J.E., 2015. Extraction of viscoelastic functions from creep data with ringing. Journal of Rheology 59. doi:10.1122/1.4904394.

[42] Ku, H., Wang, H., Pattarachaiyakoop, N., Trada, M., 2011. A review on the tensile properties of natural fiber reinforced polymer composites. Composites Part B: Engineering 42, 856 – 873. URL: http://www.sciencedirect.com/science/article/pii/S1359836811000382, doi:https://doi.org/10.1016/j.compositesb.2011.01.010.

[43] Labeeba, K., D, R., Hari, D.B.V., Durai, R., 2019a. Comprehensive Review on Potential Applications of Natural Luffa Cylindrica Fibers. pp. 02–17. doi:10.29290/PDDA.1.7.2019.2-17.

[44] Labeeba, K., Ramya, D., Vedha, B.H., Ramya, D., 2019b. Comprehensive Review on Potential Applications of Natural Luffa Cylindrica Fibers. pp. 02–17. doi:10.29290/PDDA.1.7.2019.2-17.

[45] Laidani, Y., Hanini, S., Henini, G., 2011. Use of fiber luffa cylindrica for waters traitement charged in copper. study of the possibility of its regeneration by desorption chemical. Energy Procedia 6, 381 – 388. URL: http://www.sciencedirect.com/science/article/pii/S187661021101455X, doi:https://doi.org/10.1016/j.egypro.2011.05.044. impact of Integrated Clean Energy on the Future of the Mediterranean Environment?

[46] Laidani, Y., Hanini, S., Mortha, G., Heninia, G., 2012. Study of a fibrous annual plant, luffa cylindricafor ppaper application part i: Characterization of the vegetal. Iran J Chem Chem Eng 31, 5–10. URL: http://www.ijcce.ac.ir/article_5935.html.

[47] Lee, S.Y., Yang, H.S., Kim, H.J., Jeong, C.S., Lim, B.S., Lee, J.N., 2004. Creep behavior and manufacturing parametersof wood flour filled polypropylene composites. Composite Structures 65, 459–469.

[48] Li, X., Tabil, L.G., Panigrahi, S., 2007. Chemical treatments of natural fiber for use in natural fiber-reinforced composites: A review. Journal of Polymers and the Environment 15, 25–33. URL: https://doi.org/10.1007/s10924-006-0042-3, doi:10.1007/s10924-006-0042-3.

[49] Louvier, J., Garcia-Bustos, E., Navarro, C., Mendoza-Leal, G., Alcaraz-Caracheo, L., Navarrete-Damian, J., Garcia Rodriguez, F., 2019. Tribo-mechanical behavior of hdpe/natural fibers filler composite materials 3, 3775–3781. doi:10.1557/adv.2018.644.

[50] Malkapuram, R., Kumar, V., Negi, Y.S., 2009. Recent development in natural fiber reinforced polypropylene composites. Journal of Reinforced Plastics and Composites 28, 1169–1189. URL: https://doi.org/10.1177/0731684407087759, doi:10.1177/0731684407087759, arXiv:https://doi.org/10.1177/0731684407087759.

[51] Mazali, I.O., Alves, O.L., 2005. Morphosynthesis: high fidelity inorganic replica of the fibrous network of loofa sponge (luffa cylindrica). An Acad Bras Cienc 77, 23–26. URL: https://www.scielo.br/scielo.php?script=sci_arttext&pid=S0001-37652005000100003.

[52] Mehdikhani, M., Gorbatikh, L., Verpoest, I., Lomov, S.V., 2019. Voids in fiber-reinforced polymer composites: A review on their formation, characteristics, and effects on mechanical performance. Journal of Composite Materials 53, 1579–1669. URL: https://doi.org/10.1177/0021998318772152, doi:10.1177/0021998318772152, arXiv:https://doi.org/10.1177/0021998318772152.

[53] Misra, M., s. s. ahankari, a. k. Mohanty, 2011. Creep and fatigue of natural fibre composites. Woodhead Publishing Series in Composites Science and Engineering , 289–340.

[54] Mohammed, L., 2015. A review on natural fiber reinforced polymer composite and its applications. International Journal of Polymer Science 2015, 15. doi:https://doi.org/10.1155/2015/243947.

[55] Naghdi, P.M., Murch, S.A., 1963. On the mechanical behavior of viscoelastic/plastic solids. Journal of Applied Mechanics 30, 321–328. doi:10.1115/1.3636556.

[56] Najafi, A., Najafi, S.K., 2009. Effect of load levels and plastic type on creep behavior of wood sawdust/hdpe composites. Journal of Reinforced Plastics and Composites 28, 2645–2653. URL: https://doi.org/10.1177/0731684408093320, doi:10.1177/0731684408093320, arXiv:https://doi.org/10.1177/0731684408093320.

[57] Needleman, A., Borders, T., Brinson, L., Flores, V., Schadler, L., 2010. Effect of an interphase region on debonding of a cnt reinforced polymer composite. Composites Science and Technology 70, 2207 – 2215. URL: http://www.sciencedirect.com/science/article/pii/S0266353810003477, doi:https://doi.org/10.1016/j.compscitech.2010.09.002.

[58] Nirmal, U., Hashim, J., Ahmad, M.M.H.M., 2015. A review on tribological performance of natural fibre polymeric composites. Tribology International 83, 77–104. doi:10.1016/j.triboint.2014.11.003.

[59] Ogbonna, J.C., Liu, Y.C., Liu, Y.K., Tanaka, H., 1994. Loofa (luffa cylindrica) sponge as a carrier for microbial cell immobilization. Journal of Fermentation and Bioengineering 78, 437 – 442. URL: http://www.sciencedirect.com/science/article/pii/

0922338X94900434, doi:https://doi.org/10.1016/0922-338X(94)90043-4.

[60] Papanicolaou, G., Psarra, E., Anastasiou, D., 2015. Manufacturing and mechanical response optimization of epoxy resin luffa cylindrica composite. Journal of Applied Polymer Science 132, 41992. URL: https://onlinelibrary.wiley.com/doi/abs/10.1002/app.41992, doi:https://doi.org/10.1002/app.41992.

[61] Pervaiz, M., Sain, M.M., 2003. Carbon storage potential in natural fiber composites. Resources, Conservation and Recycling 39, 325 – 340. URL: http://www.sciencedirect.com/science/article/pii/S0921344902001738, doi:https://doi.org/10.1016/S0921-3449(02)00173-8.

[62] Roble, N., Ogbonna, J., Tanaka, H., 2003. A novel circulating loop bioreactor with cells immobilized in loofa (luffa cylindrica) sponge for the bioconversion of raw cassava starch to ethanol. Applied Microbiology and Biotechnology 60, 671–678. URL: https://doi.org/10.1007/s00253-002-1119-0, doi:10.1007/s00253-002-1119-0.

[63] Saeed, A., Iqbal, M., 2013. Loofa (luffa cylindrica) sponge: Review of development of the biomatrix as a tool for biotechnological applications. Biotechnology Progress 29, 573–600. URL: https://aiche.onlinelibrary.wiley.com/doi/abs/10.1002/btpr.1702, doi:10.1002/btpr.1702, arXiv:https://aiche.onlinelibrary.wiley.com/doi/pdf/10.1002/btpr.1702.

[64] Saw, S., Purwar, R., Nandy, S., Ghose, J., Sarkhel, G., 2013. Fabrication, characterization, and evaluation of luffa cylindrica fiber reinforced epoxy composites. BioResources 8, 4805–4826. URL: https://ojs.cnr.ncsu.edu/index.php/BioRes/article/view/BioRes_08_4_4805_Saw_Luffa_cylindrica_Fiber.

[65] Scott, D.W., Lai, J.S., Zureick, A.H., 1995. Creep behavior of fiber-reinforced polymeric composites: A review of the technical literature. Journal of Reinforced Plastics and Composites 14, 588–617. URL: https://doi.org/10.1177/073168449501400603, doi:10.1177/073168449501400603, arXiv:https://doi.org/10.1177/073168449501400603.

[66] Seki, Y., 2009. Innovative multifunctional siloxane treatment of jute fiber surface and its effect on the mechanical properties of jute/thermoset composites. Materials Science and Engineering: A 508, 247 – 252. URL: http://www.sciencedirect.com/science/article/pii/S0921509309000690, doi:https://doi.org/10.1016/j.msea.2009.01.043.

[67] Sgriccia, N., Hawley, M., Misra, M., 2008. Characterization of natural fiber surfaces and natural fiber composites. Composites Part A: Applied Science and Manufacturing 39, 1632 – 1637. URL: http://www.sciencedirect.com/science/article/pii/S1359835X08001899, doi:https://doi.org/10.1016/j.compositesa.2008.07.007.

[68] Shen, J., Xie, Y.M., Huang, X., Zhou, S., Ruan, D., 2012. Mechanical properties of luffa sponge. Journal of the Mechanical Behavior of Biomedical Materials 15, 141 – 152. URL: http://www.sciencedirect.com/science/article/pii/S1751616112001993, doi:https://doi.org/10.1016/j.jmbbm.2012.07.004.

[69] Shen, J., Xie, Y.M., Huang, X., Zhou, S., Ruan, D., 2013. Behaviour of luffa sponge material under dynamic loading. International Journal of Impact Engineering 57, 17 – 26. URL: http://www.sciencedirect.com/science/article/pii/S0734743X13000110, doi:https://doi.org/10.1016/j.ijimpeng.2013.01.004.

[70] Shen, W., Shao, J., 2014. A micro-macro model for porous geomaterials with inclusion debonding. International Journal of Damage Mechanics , 1–21doi:10.1177/1056789514560915.

[71] Siqueira, G., Bras, J., Follain, N., Belbekhouche, S., Marais, S., Dufresne, A., 2013. Thermal and mechanical properties of bio-nanocomposites reinforced by luffa cylindrica cellulose nanocrystals. Carbohydrate Polymers 91, 711 – 717. URL: http://www.sciencedirect.com/science/article/pii/S0144861712008314, doi:https://doi.org/10.1016/j.carbpol.2012.08.057.

[72] Tabi, T., Bakonyi, P., Hajba, S., Herrera-Franco, P., Czigany, T., Kovacs, J., 2016. Creep behaviour of injection-moulded basalt fibre reinforced poly(lactic acid) composites. Journal of Reinforced Plastics and Composites , 1–11.

[73] Tanobe, V.O., Sydenstricker, T.H., Munaro, M., Amico, S.C., 2005. A comprehensive characterization of chemically treated brazilian

sponge-gourds (luffa cylindrica). Polymer Testing 24, 474 – 482. URL: http://www.sciencedirect.com/science/article/pii/S014294180500005X, doi:https://doi.org/10.1016/j.polymertesting.2004.12.004.

[74] Thakur, V.K., Thakur, M.K., 2014. Processing and characterization of natural cellulose fibers/thermoset polymer composites. Carbohydrate Polymers 109, 102 – 117. URL: http://www.sciencedirect.com/science/article/pii/S0144861714002719, doi:https://doi.org/10.1016/j.carbpol.2014.03.039.

[75] Thanikachalam, J., Vasiraja, N., v Vignesh, 2018. Evaluation on properties of industrial workers safety helmet using natural hybrid composite, in: SAE Technical Paper, SAE International. URL: https://doi.org/10.4271/2018-28-0049, doi:10.4271/2018-28-0049.

[76] Vilaplana, F., Stromberg, E., Karlsson, S., 2010. Environmental and resource aspects of sustainable biocomposites. Polymer Degradation and Stability 95, 2147 – 2161. URL: http://www.sciencedirect.com/science/article/pii/S0141391010003101, doi:https://doi.org/10.1016/j.polymdegradstab.2010.07.016. 2nd International Conference on Biodegradable Polymers and Sustainable Composites - Alicante 2009.

[77] van Voorn, B., Smit, H., Sinke, R., de Klerk, B., 2001. Natural fibre reinforced sheet moulding compound. Composites Part A: Applied Science and Manufacturing 32, 1271 – 1279. URL: http://www.sciencedirect.com/science/article/pii/S1359835X01000859, doi:https://doi.org/10.1016/S1359-835X(01)00085-9.

[78] Wambua, P., Ivens, J., Verpoest, I., 2003. Natural fibres: can they replace glass in fibre reinforced plastics? Composites Science and Technology 63, 1259 – 1264. URL: http://www.sciencedirect.com/science/article/pii/S0266353803000964, doi:https://doi.org/10.1016/S0266-3538(03)00096-4. eco-Composites.

[79] Xie, Y., Hill, C.A., Xiao, Z., Militz, H., Mai, C., 2010. Silane coupling agents used for natural fiber/polymer composites: A review. Composites Part A: Applied Science and Manufacturing 41, 806 – 819. URL: http://www.sciencedirect.com/science/article/pii/S1359835X10000850, doi:https://doi.org/10.1016/j.compositesa.2010.03.005.

[80] Zampieri, A., Mabande, G.T., Selvam, T., Schwieger, W., Rudolph, A., Hermann, R., Sieber, H., Greil, P., 2006. Biotemplating of luffa cylindrica sponges to self-supporting hierarchical zeolite macrostructures for bio-inspired structured catalytic reactors. Materials Science and Engineering: C 26, 130 – 135. URL: http://www.sciencedirect.com/science/article/pii/S0928493105002808, doi:https://doi.org/10.1016/j.msec.2005.08.036.

[81] Zhao, Y., Weng, G., 1996. Plasticity of a two-phase composite with partially debonded inclusions. International Journal of Plasticity 12, 781 – 804. URL: http://www.sciencedirect.com/science/article/pii/S0749641996000290, doi:https://doi.org/10.1016/S0749-6419(96)00029-0.